

Crystallization and magnetic properties of amorphous iron–chromium oxide nanoparticles synthesized by sonochemistry

This article has been downloaded from IOPscience. Please scroll down to see the full text article.

2012 Adv. Nat. Sci: Nanosci. Nanotechnol. 3 015017

(<http://iopscience.iop.org/2043-6262/3/1/015017>)

View [the table of contents for this issue](#), or go to the [journal homepage](#) for more

Download details:

IP Address: 123.27.12.208

The article was downloaded on 19/03/2012 at 16:54

Please note that [terms and conditions apply](#).

Crystallization and magnetic properties of amorphous iron–chromium oxide nanoparticles synthesized by sonochemistry

Dang Phu Nguyen, Quoc Tuan Tran, Xuan Sy Trinh, Thanh Cao Hoang, Hoang Nam Nguyen and Hoang Hai Nguyen

Center for Materials Science, Faculty of Physics, Hanoi University of Science, Vietnam National University, 334 Nguyen Trai, Thanh Xuan, Hanoi, Vietnam

E-mail: namnh@hus.edu.vn

Received 10 October 2011

Accepted for publication 6 January 2012

Published 14 March 2012

Online at stacks.iop.org/ANSN/3/015017

Abstract

Amorphous iron–chromium oxide $\text{Fe}_{2-x}\text{Cr}_x\text{O}_3$ ($x = 0, 0.05, 0.10, 0.15, 0.20$) nanoparticles were synthesized by sonochemical method at 80°C . Crystallization process of the annealed samples showed a strong ferromagnetic behavior due to the existence of the maghemite phase. The effect of chromium replacing iron in the crystallization process of $\text{Fe}_{2-x}\text{Cr}_x\text{O}_3$ nanoparticles was systematically studied by adjusting initial concentration of Cr^{3+} . The activation energy of the samples deduced from thermal analysis and increased with doping chromium showed that the existence of chromium can significantly slow down the ageing effect of the amorphous iron oxide.

Keywords: crystallization process, amorphous iron oxide, sonochemistry, phase transition, magnetic properties.

Classification number: 5.02

1. Introduction

Iron oxide nanoparticles have attracted much interest because of their wide application abilities in biological separation [1], drug delivery [2], magnetic liquids [3], diagnostic imaging [4], solar energy transformation [5, 6], magnetic devices [7] and the electronics industry [8]. Amorphous iron oxide nanoparticles having a large surface area with a large number of unsaturated bonds, leads to them being very good candidates for catalytic activities [9, 10] as well as sensors [11]. Amorphous iron oxide nanoparticles have been synthesized by various methods such as electrochemical [12], microwave heating [13], but the most popular method to synthesize them is sonochemistry [14–16]. Amorphous formation requires a high cooling rate and the sonochemical technique can produce a cooling rate of more than ten million degrees per second [17].

Understanding the crystallization process of amorphous iron oxide nanoparticles is important for applications. The

amorphous state is metastable and changes to the crystalline state via crystallization process, during which a long-range order can be formed and the physical and chemical properties of materials should change accordingly. The crystallization process does not occur at a unique temperature but hinges on temperature and time. Usually, one determines the crystallization temperature from thermal analyses where the crystallization rate reaches maximum. At lower temperatures, the crystallization process happens with much lower rates, which used to be ignored in experiments. From the viewpoint of application abilities, the stability of materials under ambient conditions is important. In other words, the change of properties of materials with time, i.e. the ageing effects should be well investigated. In a previous report, the crystallization as well as the magnetic properties of iron oxide nanoparticles prepared by sonochemical method were reported [18], but the ageing effects and how to overcome them were not proposed. In this article, chromium was introduced into amorphous iron oxide nanoparticles to slow down the ageing

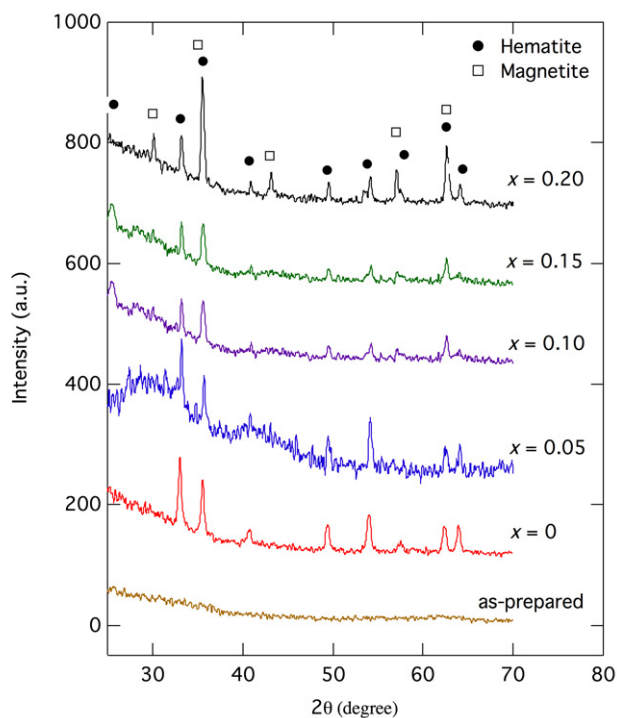


Figure 1. XRD pattern of as-prepared $\text{Fe}_{2-x}\text{Cr}_x\text{O}_3$ sample and sample annealed at 600°C with various content x of chromium.

Table 1. Chemical composition of the as-prepared $\text{Fe}_{2-x}\text{Cr}_x\text{O}_3$. The error bond in composition is $\pm 0.5\%$. The lattice parameters a and c are of the corundum type structure of the hematite phase.

Sample	1	2	3	4	5
x	0	0.05	0.10	0.15	0.20
Concentration from EDS	0	0.06	0.098	0.17	0.24
a (Å)	5.045	5.042	5.039	5.036	5.035
c (Å)	13.068	13.067	13.065	13.063	13.062

effect. We systematically investigated the crystallization and magnetic properties of the iron-chromium oxide nanoparticles by changing the content of chromium.

2. Experimental

The process of synthesis of amorphous iron–chromium oxide $\text{Fe}_{2-x}\text{Cr}_x\text{O}_3$ nanoparticles by sonochemical reaction has been described elsewhere [18] with some modifications. Briefly, 80 ml solution of a 0.01 M ferric chloride $\text{FeCl}_3 \cdot 6\text{H}_2\text{O}$, 1 weight percent polyethyleneglycol 2000, 1 M urea and $\text{Cr}(\text{NO}_3)_3 \cdot 9\text{H}_2\text{O}$ was prepared in a 150 ml flask. The composition ratio of chromium $x = 0, 0.05, 0.10, 0.15, 0.20$ was controlled by the amount of added $\text{Cr}(\text{NO}_3)_3 \cdot 9\text{H}_2\text{O}$. The solution in the flask was ultrasonicated with a power of 400 W and frequency of 20 kHz emitted by a Sonic VCX 750 ultrasound emitter in 4 h. The temperature of reaction was kept at 80°C . The reacted solution was cooled down to room temperature and amorphous iron-chromium oxide powder was collected by using a centrifuge. After washing five times with distilled water and air-drying at 75°C , the final samples were then subjected for further characterization.

The thermal behavior of the as-prepared powder was investigated by STD 2960 differential scanning calorimetry

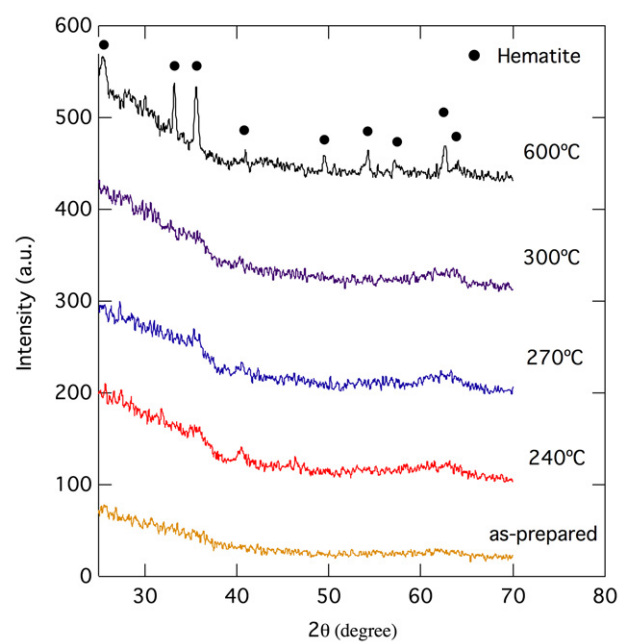


Figure 2. XRD patterns of sample with $x = 0.10$ after annealed at temperature of 240, 270, 300 and 600°C .

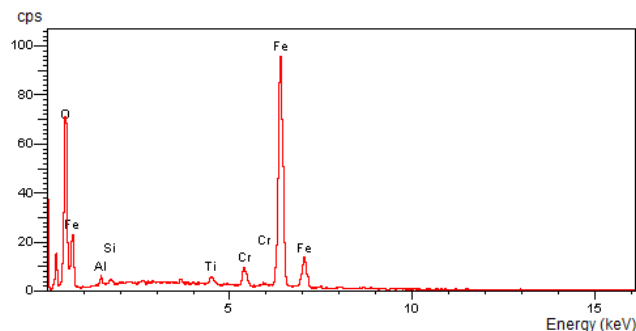


Figure 3. EDS spectra of sample with $x = 0.10$.

(DSC) with different heating rates of $10\text{--}30^\circ\text{C min}^{-1}$ in air over the temperature range of $25\text{--}600^\circ\text{C}$. In this report, the as-prepared sample was annealed at various temperatures from 200°C to 600°C in order to investigate the crystallization process. The phase composition of the as-prepared powder and the annealed samples at different temperatures were studied by x-ray diffractometer Bruker D5005 and energy dispersive spectroscopy (EDS) measurements. The morphology of samples was investigated by a S4800-Hitachi field emission scanning electron microscope (FE-SEM). Magnetic properties of samples were measured by using DMS-880 vibrating sample magnetometer (VSM).

3. Results and discussion

The x-ray diffractograms measured on the as-prepared powder and the iron-chromium oxide powders with various x after annealed at 600°C for 30 min are presented in figure 1. The broad x-ray peak below 30° is due to the amorphous nature scattered from the glass plate that was used as the sample holder in the x-ray diffraction (XRD) experiments. The as-prepared samples show the typical amorphous structure on XRD patterns. After annealing, all the samples showed the

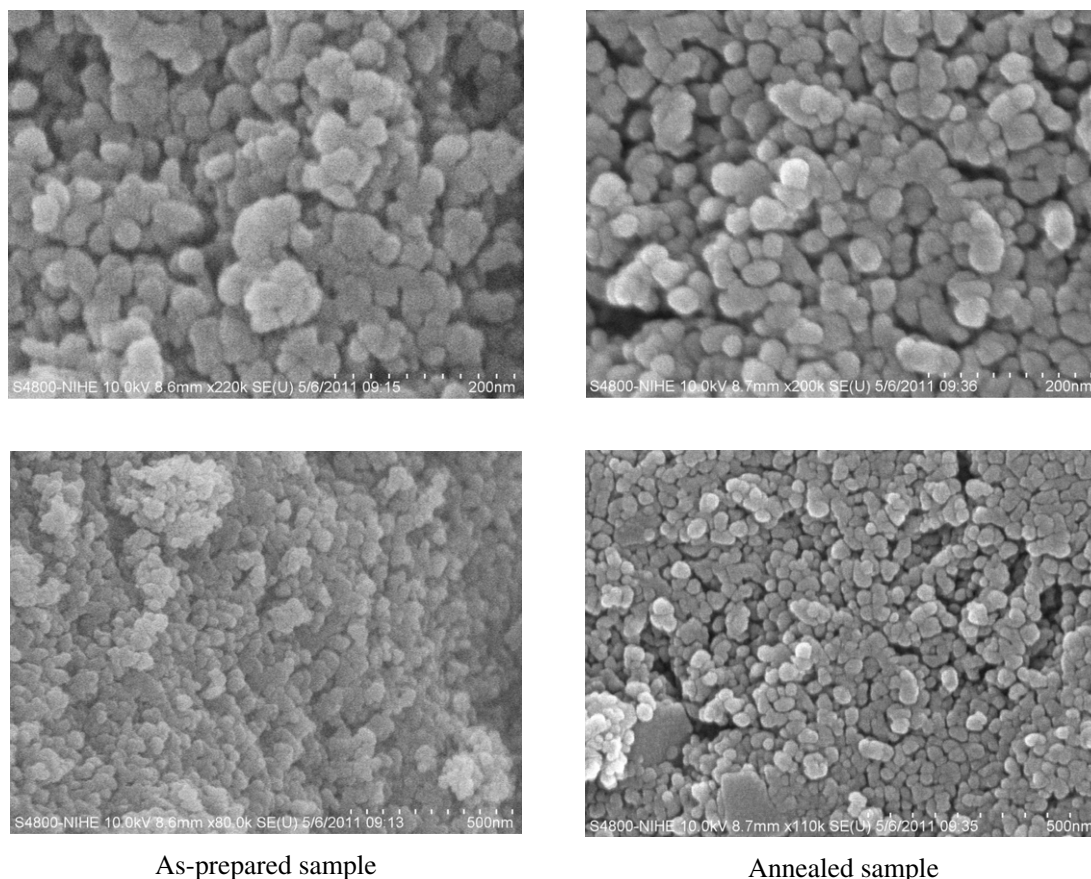


Figure 4. FE-SEM images of the sample with $x = 0.10$.

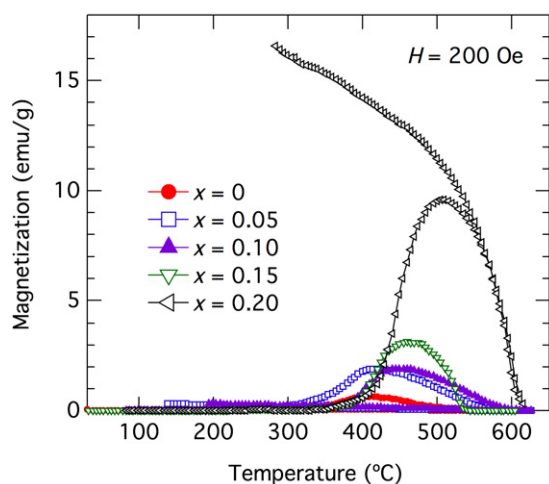


Figure 5. Temperature dependence of magnetization under the applied field of 200 Oe of the iron-chromium oxide nanoparticles $Fe_{2-x}Cr_xO_3$ with various x .

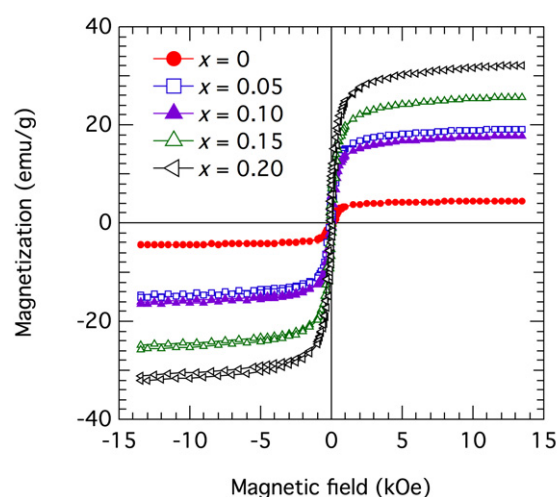


Figure 6. Magnetic field dependence of the magnetization at room temperature of samples with various x after annealing to high temperature.

presence of the hematite Fe_2O_3 phase (JCPDS 73-2234). The sample with $x = 0.20$ showed the coexistence of the hematite Fe_2O_3 and the magnetite Fe_3O_4 phases (JCPDS 79-0418). The lattice parameters of the corundum type structure deduced from the XRD results are shown in table 1. Both the lattice parameters a and c decreased slightly with increasing the chromium content. This can be understood by the decrease of ionic radius when iron ions were replaced by chromium ion in their lattice [19]. Figure 2 presents the XRD diffractograms

of the sample with $x = 0.10$ at various annealed temperatures. The broad and weak peaks shown in XRD patterns indicated that the crystallization gradually processed upon annealing up to $300^\circ C$. The diffraction peak at 41.2° can be assigned to the α - Fe_2O_3 structure while peaks at 35.6 and 62.5° can be assigned to either the α - Fe_2O_3 or γ - Fe_2O_3 one (JCPDS 39-1346). With increasing annealed temperature to $600^\circ C$, the sample showed clear diffraction peaks of the hematite phase.

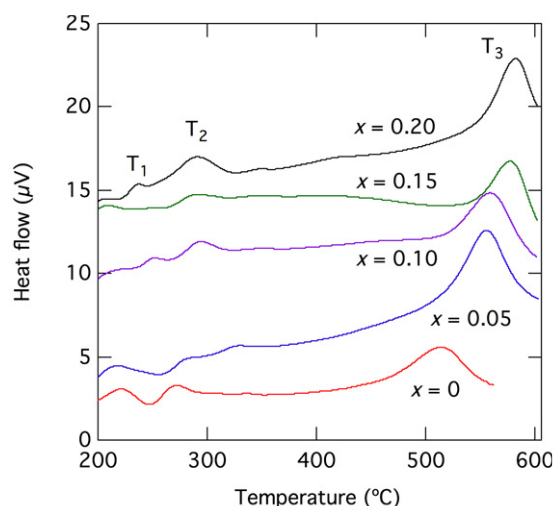


Figure 7. DSC data of the sample with various Cr contents x .

The composition of chromium in samples was controlled by the amount of initial added $\text{Cr}(\text{NO}_3)_3 \cdot 9\text{H}_2\text{O}$ and was determined from EDS data. Typically, the EDS analysis of the sample with $x = 0.10$ is shown in figure 3 and the results of the EDS analyses are shown in table 1. The chromium concentration in the as-prepared sample is almost equal to the concentration of the precursors.

The morphology of the as-prepared samples and the sample with $x = 0$ annealed at 600°C investigated by transmission electron microscopy (TEM) [18] shows that the particle size increased from ~ 5 nm for the unannealed sample to ~ 22 nm for the annealed sample. In this report, we investigated the morphology of the sample with $x = 0.10$ by FE-SEM. The results are shown in figure 4. It also can be seen that the size of sample increased after annealing, however, the differences are not clear.

The temperature dependence of the magnetization under a magnetic field of 200 Oe of the iron-chromium samples is shown in figure 5. The heating curve started from room temperature where amorphous as-prepared samples were in non-ferromagnetic state. In this state, long-ranged order of the magnetic moment of Fe and Cr ions was not present. Therefore, the samples did not show ferromagnetic interaction. For the sample with $x = 0$, the magnetization showed a sudden increase at around 230°C , reached a maximum of 0.61 emu g^{-1} at 414°C , then decreased to almost zero at high temperature around 600°C . The strong increase at above 230°C suggests that the crystallization process of a ferromagnetic phase occurs at those temperatures. Above 600°C , thermal agitation dominated the ferromagnetic interaction, at which point the sample was non-ferromagnetic. The cooling curve starting at 600°C back to room temperature was monotonically increasing with temperature. The samples with $x = 0.05, 0.10$ and 0.15 behaved similarly with one peak of magnetization, but the onset temperature of the peak slightly increased with increasing x . The sample with $x = 0.20$, however, has different behavior with very high magnetization of 9.6 emu g^{-1} at the maximum of the magnetization peak located at about 510°C . After cooling from 600°C , the magnetization curve at room temperature of samples with various x were measured, as shown in

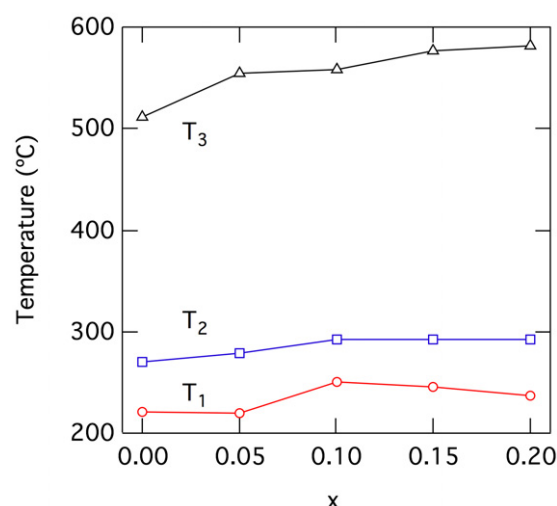


Figure 8. Changes in the temperature at which the exothermic peaks of $\text{Fe}_{2-x}\text{Cr}_x\text{O}_3$ became maximum as increasing x .

figure 6. All of the samples show ferromagnetic interaction. The saturated magnetization increases with the content of chromium. The sample with $x = 0$ shows a small value of saturated magnetization of 4.4 emu g^{-1} . Upon doping Cr into sample, the saturated magnetization increases significantly to 15.1, 17.1 and 25.7 emu g^{-1} for samples with $x = 0.05, 0.10$ and 0.15 , respectively. The sample with $x = 0.20$ shows the highest saturated magnetization of 32.1 emu g^{-1} .

The crystalline iron oxides are maghemite $\gamma\text{-Fe}_2\text{O}_3$, hematite $\alpha\text{-Fe}_2\text{O}_3$ or magnetite Fe_3O_4 . The maghemite is ferrimagnetic with saturation magnetization of 60 emu g^{-1} . The hematite is antiferromagnetic and sometimes has low saturation magnetization of about a few emu g^{-1} [20] or sometimes has high saturation magnetization [21]. The origin of the ferromagnetic property of hematite was explained by the disorders in the materials or a large number of point defects, which was demonstrated by Raman spectroscopy [18, 20, 21]. The magnetite has the highest saturation magnetization of 80 emu g^{-1} . Because the XRD data of samples with $x = 0, 0.05, 0.10, 0.15$ after cooling down from 600°C consists only of the hematite phase and the magnetite phase does not exist, the crystallized ferromagnetic phase in these samples can be assigned to the maghemite phase $\gamma\text{-Fe}_2\text{O}_3$. At the end of the peaks of magnetization on heating curves of these samples presented in figure 6, there is a transition from maghemite $\gamma\text{-Fe}_2\text{O}_3$ to hematite $\alpha\text{-Fe}_2\text{O}_3$. The XRD pattern of sample $x = 0.20$, however, consists of the magnetite as well as the hematite phase. The high value of magnetization of sample $x = 0.20$ during heating can be explained by the co-existence of the magnetite phase with the maghemite phase at high temperature. The maghemite phase then changed to hematite phase at higher temperature but the magnetite phase did not. After cooling down from high temperature to room temperature, this sample showed the co-existence of magnetite as well as hematite phase resulting in high value of saturation magnetization at room temperature.

The thermal behavior of samples with various x investigated by DSC measurements is shown in figure 7. Increasing x led to the increase of all exothermic peaks. The value of T_1 and T_2 changed strongly when x reached up to 0.10

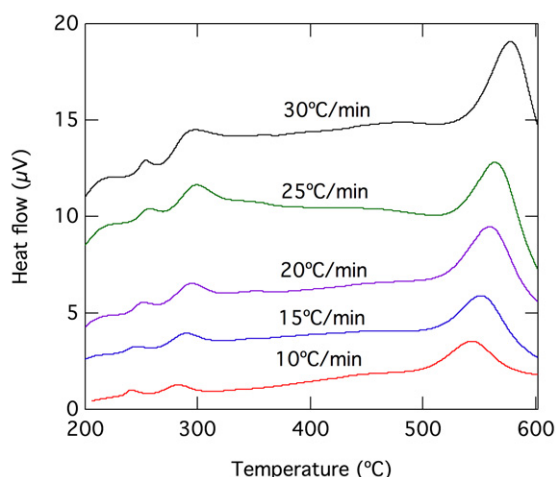


Figure 9. DSC data of sample $x = 0.10$ with the heating rate of $10\text{--}30\text{ }^{\circ}\text{C min}^{-1}$.

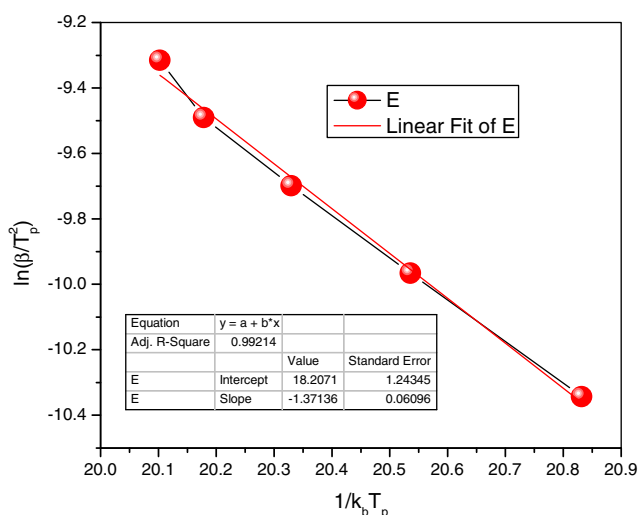


Figure 10. The activation energy calculation with the Kissinger model for the sample $x = 0.10$.

while the values of T_3 kept increasing in the whole range of x as shown in figure 8. We expect that the activation energy of the amorphous iron-chromium oxide samples increases with the content of chromium. Figure 9 presents the dynamic process of the sample $x = 0.10$ with the heating rates of $10\text{--}30\text{ K min}^{-1}$. Comparing to the sample with $x = 0$, all the exothermic peaks of sample $x = 0.10$ occurred at higher temperatures. Using the Kissinger model [22], the activation energies corresponding to the second peak were estimated as shown in figure 10. Accordingly, the activation energies E_a of the peak T_1 , T_2 and T_3 of the sample with $x = 0.10$ are 140, 156 and 170 kJ mol^{-1} while these values of sample $x = 0$ are 105, 130 and 186 kJ mol^{-1} , respectively. In order to investigate the ageing effect of the amorphous iron-chromium oxide materials, the activation energy of the first peaks is important. The time of completing the crystallization can be express as $t \propto \exp(E_a/RT)$ which shows that the rate of crystallization at room temperature is much lower than that at T_1 . In the sample with $x = 0$, if the time of reaction at T_1 is in the order of a few seconds, then the reaction time at room temperature is around a year. Using the above values of the activation energy for peak T_1 , one can estimate the reaction

time at T_1 of sample $x = 0.10$, which is around 15 years or increases around 15 times.

4. Conclusion

Amorphous iron–chromium oxide nanoparticles have been prepared by sonochemistry. The crystallization process and magnetic properties were investigated systematically with the content of Cr. The ageing effect of the amorphous iron oxide materials can be slowed down with the presence of Cr by a factor of 15 times.

Acknowledgments

This work was financially supported by the National Foundation of Science and Technology Development (NAFOSTED Grant No 103.02.68.09) and the key project QGTD.10.29 of Vietnam National University in Hanoi. The authors would like to thank Professor Gubicza Jenő for the useful discussion.

References

- [1] Leslie-Pelecky D L, Labhasetwar V and Kraus R H 2005 Nanobiomagnetics *Advanced Magnetic Nanostructure* ed D J Sellmyer and R S Skomski (New York: Kluwer)
- [2] Thach C V, Hai N H and Chau N 2008 *J. Korean Phys. Soc.* **52** 1332
- [3] Rosenzweig R E 1985 *Ferrohydrodynamics* (Cambridge: Cambridge University Press)
- [4] Berry C C and Curtis A S G 2003 *J. Phys. D: Appl. Phys.* **36** R198
- [5] Machala L, Zboril R and Gedanken A 2007 *J. Phys. Chem. B* **111** 4003
- [6] Danzfuß B and Stimming U 1984 *J. Electroanal. Chem.* **164** 89
- [7] Casas L, Roig A, Rodriguez E, Molins E, Tejada J and Sort J 2001 *J. Non-Cryst. Solids* **285** 37
- [8] Zboril R, Mashlan M and Petridis D 2002 *Chem. Mater.* **14** 969
- [9] Perkas N, Koltypin Y, Palchik O, Gedanken A and Chandrasekaran S 2001 *Appl. Catal. A* **209** 125
- [10] Srivastava D N, Perkas N, Gedanken A and Felner I 2002 *J. Phys. Chem. B* **106** 1878
- [11] Neri G, Bonavita A, Milone C, Pistone A and Galvagno S 2003 *Sensors Actuators B* **92** 326
- [12] Pascal C, Pascal J L, Favier F, Elidrissi Moubtassim M L and Payen C 1999 *Chem. Mater.* **11** 141
- [13] Liao X, Zhu J, Zhong W and Chen H Y 2001 *Mater. Lett.* **50** 341
- [14] Pinkas J, Reichlova V, Zboril R, Moravec Z, Bezdiccka P and Matejkova J 2008 *Ultrason. Sonochem.* **15** 257
- [15] Srivastava D N, Perkas N, Gedanken A and Felner I 2002 *J. Phys. Chem. B* **106** 1878
- [16] Shafi K V P M, Ulman A, Yan X, Yang N-L, Estournes C, White H and Rafailovic M 2001 *Langmuir* **17** 5093
- [17] Suslick K S, Choe S B, Cichowlas A A and Grinstad M W 1991 *Nature* **353** 414
- [18] Phu N D, Sy T X, Cao H T, Nam N H and Hai N H 2012 *J. Non-Cryst. Solids* **358** 537
- [19] Levinstein H, Robbins M and Capio C 1972 *Mater. Res. Bull.* **7** 27
- [20] Ramesh R, Ashok K, Bhalero G M, Ponnusamy S and Muthamizhchel-van C 2010 *Cryst. Res. Technol.* **45** 965
- [21] Wu J, Mao S, Ye Z-G, Xie Z and Zheng L 2010 *Appl. Mater. Interfaces* **2** 1561
- [22] Kissinger H E 1957 *Anal. Chem.* **29** 1702